High-Frequency Analysis of Scattering from Complex Targets in Half Space

Xiao Feng Li , Yong Jun Xie , Rui Yang , and Yuan Yuan Wang

National Key Laboratory of Antennas and Microwave Technology,
Xidian University, Xi'an 710071, China
lxf.xidian@yahoo.com.cn , yjxie@xidian.edu.cn , mattomato811118@yahoo.com.cn ,
wylpforever@163.com

***Abstract*—** The high-frequency method for solving the scattering from electrically large conductive targets in half space is presented in this paper. The high-frequency method is deduced by introducing the half-space Green's function into the conventional method of physical optics, method of equivalent currents. Combined with the graphical-electromagnetic computing method and ray tracing technique that account for shadowing and multiple scattering in half space, one may calculate the radar cross-section of a conductive target object in a half space. The numerical results show that this method is efficient and accurate.

***Index Terms*—** Half-space physical optics (HFPO), half-space Equivalent Edge Currents (HFEEC), graphical-electromagnetic computing, radar cross section (RCS).

I. INTRODUCTION

With the development of electromagnetics, researchers have directed significant attention toward targets in half space, especially the electrically large PEC targets above the earth or the sea, such as geophysical, remote sensing, wave propagation. A variety of RCS prediction softwares have been widely used for interactive modeling, design, and analysis of aircraft with RCS specifications in free space [1], which are based on the high-frequency techniques [2-7] and provide an efficient tool to obtain real-time results. However, how fast and accurate it is to calculate the radar cross section of half-space targets is still a challenging problem, in particular, the objectives of great size.

Numerous authors have derived a variety of methods which are used for computing the radar cross section (RCS) of complex radar targets in half space. The scattering fields of the targets in half space could be computed by using the Finite element method (FEM) [8], Finite-difference time-domain methods (FDTD) [9], but they cause some difficulties in the solution procedure such as the discrete space need for a huge number of grids in the solution procedure [10]. Some researchers try to combine the half-space Green's function with the Method of moment (MOM), or fast multipole method (FMM) to consider the electrically large targets in half space [11], but this also requires more mass storage memory in general personal computer, which results in lower processing speed and more computing time.

In addition, Johnson and others clarify an accuracy of a "four-path" model which includes single scattering effects only [12]. The results show that the four-path model provides reasonable predictions. The above methods have provided us with a better idea to solve the targets in half space.

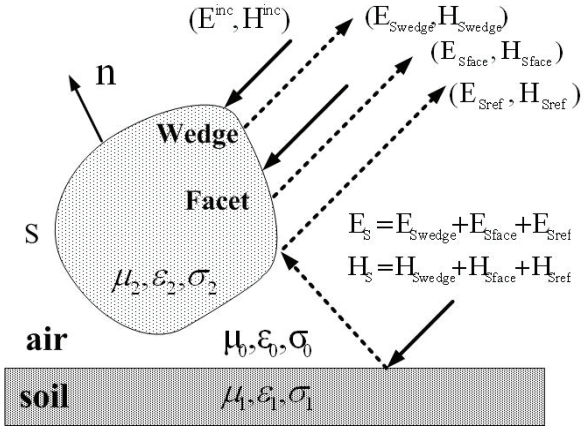

Fig. 1. a plane wave illuminating an arbitrarily shaped 3-D object located above a lossy half space.

In this paper, an improved high-frequency method is presented for analysis of scattering from

electrically large targets in a half space. Based on the analysis of the scattered field due to the facet's surface in half space [13-14], we have further introduced the high-frequency method into the wedges of conductive targets with electrically large size in half space. Furthermore, the facets illuminated by the ground reflected wave were also added to the contributions from the firstly illuminated facets. Therefore, inclusion of returns from these in the overall return is an important process, and one should be aware of their magnitude.

II. THEORY

As shown in Fig. 1, consider an arbitrarily shaped object illuminated by a plane wave in a half space, and surface *S* is assumed to represent a closed surface of a target.

This paper deals with RCS analysis where it is implicitly assumed that the radar frequency is high enough such that the corresponding wavelength is small compared to the physical dimensions of the scattering body. Therefore we use the term complex body to imply also a body with large electric dimensions. Thus the scattering calculations are in the high-frequency region. Due to the poor rate of convergence of the moment method when applied to electrically large bodies (in addition to its requirement for a large computer), it is logical to use the high-frequency method.

The classical high-frequency techniques for RCS prediction are based on a target model in terms of facets and wedges [1]. Besides we included the correction in our calculations by accounting for the currents that are induced on a target that was illuminated by the ground reflected wave. Thus, the term for the overall scattered field from a complex body may be written as:

Total scattered field E_s = scattered fields from facets E_{sface} + scattered fields from wedges E_{swedge} + scattered fields from ground reflected wave E_{sref}

When calculating these fields, one may precede by using magnetic or electric field integral equation formulations. The following calculations are presented in terms of electric field formulations.

A. Graphical Processing in Half-Space

The GRECO method was introduced by Rius in 1993 [3]. It can be integrated with CAD geometric modeling packages and high-frequency theory for RCS predictions. Using the hardware graphics accelerator, hidden surfaces of the image have been previously removed.

To the fixed screen, the calculation complexity is not varied with the complexity and dimension of targets. The targets are rebuilt by displaying lists technology of OpenGL and hidden surfaces of the image have been previously removed by the hardware graphics accelerator. Then we make use of the resolution to disperse the curve face into pixels that satisfy the requirement of the electromagnetic calculation, meanwhile, the scene is rendered using the Phong local illumination model [3].

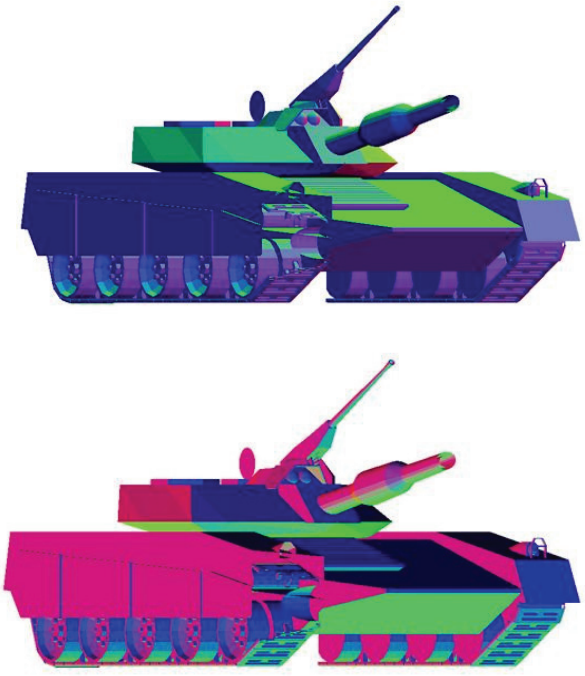

Fig. 2. Rendered image of tank in half space at the workstation screen. Six red, blue, and green light sources are located on positive and negative axis. The blending of the three colors at each pixel of the two images is equal to the positive and negative components of the unit normal.

For three light sources of purely green, red and blue colors, respectively, located over each one of the three coordinate axes, the three color components for this pixel are equal to the

(n_x, n_y, n_z) components of the unit normal to surface.

As shown in Fig. 3, in order to show that this method is efficient and accurate, we have returned to the calculated unit normal on the surface and have a good agreement with actual results. Meanwhile, the depths of each pixel are obtained in the same way. The depth of each pixel is equal to the distance between the observer and each surface element.

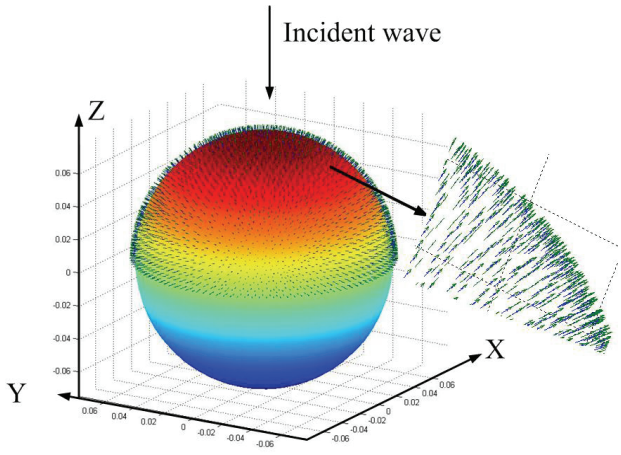

Fig. 3. Calculated unit normal distribution of the sphere in half space. The incident wave direction is $\theta_{inc} = 0, \varphi_{inc} = 0$.

Edges are detected on the target image as discontinuities of the unit normal to the surface when the z coordinates remain continuous. It must be noted that eclipsed surfaces may also produce discontinuities in the normal to the surface, but in that case the z coordinate would be discontinuous.

Obtaining the unit normal and edge parameters of each illuminated pixel of the target, the radar cross section of conductive targets can be exactly calculated with the half-space high frequency method.

B. Facet Scattering in Half-Space

The scattered electric field $\mathbf{E}_{sf}$ from an arbitrary facet is based on the following form for the electric field integral equation.

$$\mathrm{E}_{sf}(r) = -\mathbf{j}\omega \mathrm{A}(r) - \nabla V_e, , r \in S\,, \qquad (1)$$

where A and V_e represent electric vector and scalar potentials.

According to the high-frequency theory, we can get the accurate surface current by applying physical optics approximations over illuminated surface in half space. Through the proper boundary conditions, the surface current can be represented as:

$$\mathbf{J}(\bar{\mathbf{r}}') \approx 2\hat{\mathbf{n}} \times \mathbf{H}_{\mathbf{i}}\,, \qquad (2)$$

where $\hat{n}$ is the inward surface unit normal and $\mathbf{H}_{\mathbf{i}}$ is the polarization unit vectors for incident magnetic field.

In order to solve the scattering fields of the electrically large PEC targets in half space, the half-space Green's function was introduced into the high-frequency method. The half-space Green's function can be impressed by the vector and scalar potentials, and the vector potential is not uniquely specified. In this paper, we express it as follows [15]:

$$\overline{\mathbf{G}}_A = (\hat{\mathbf{x}}\hat{\mathbf{x}} + \hat{\mathbf{y}}\hat{\mathbf{y}})G_A^{xx} + \hat{\mathbf{z}}\hat{\mathbf{x}}G_A^{zx} + \hat{\mathbf{z}}\hat{\mathbf{y}}G_A^{zy} + \hat{\mathbf{z}}\hat{\mathbf{z}}G_A^{zz} \qquad (3)$$

with

$$G_A^{xx} = G_A^{yy}\,,\ G_x^{qe} = G_y^{qe}\,. \qquad (4)$$

Here, G_A^{xx}, G_A^{zx}, G_A^{zy} and G_A^{zz} denote the spatial domain half-space Green's function for the electric vector potentials; G_x^{qe}, G_y^{qe} and G_z^{qe} denote the spatial domain half-space Green's function for the electric scalar potentials.

In order to obtain the half-space Green's function, we compute the vector and the scalar potentials by the discrete complex image method. Through the Sommerfeld identity, a closed-form spatial Green's function of a few terms is found from the quasi-dynamic images, the complex images, and the surface waves [15-16].

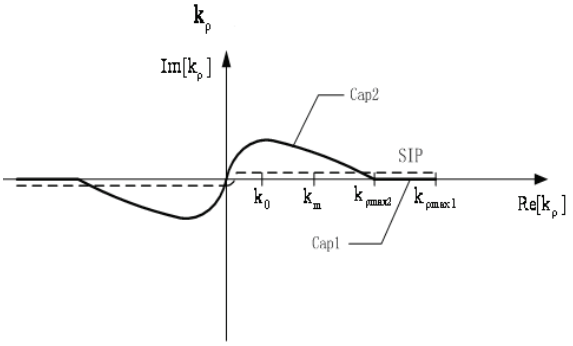

Fig. 4. The paths *Cap*1 and *Cap*2 used in two-level approximation.

To obtain the spatial-domain Green's functions in closed forms, it would be useful to give the definition of the spatial-domain Green's function

$$G = \frac{1}{4\pi}\int_{SIP} \widetilde{G}(k_\rho) H_0^{(2)}(k_\rho) k_\rho dk_\rho , \qquad (5)$$

where, G and $\widetilde{G}$ are the Green's function in the spatial and spectral domains, respectively. $H_0^{(2)}$ is the Hankel function of the second kind and *SIP* is the Sommerfeld integration path.

To alleviate the necessity of investigating the spectral-domain Green's functions in advance and the difficulties caused by the trade-off between the sampling range and the sampling period, the approximation is performed in two levels. The first part of approximation is performed along the path *Cap*1 while the second part is done along the path *Cap*2 as shown in Fig.4. The main formulations may refer to [17-18].

It is permissible to express the vector and the scalar potentials as follows:

$$A(r) = \mu_0 \int_S \overline{G}_A(r,r') \cdot J(r') dS' \qquad (6)$$

$$V_e(r) = \frac{-1}{j\omega\omega_0}\int_S [G_x^{qe}(r,r')\frac{\partial J_x}{\partial x'} + G_y^{qe}(r,r')\frac{\partial J_y}{\partial y'} + G_z^{qe}(r,r')\frac{\partial J_z}{\partial z'}] dS' , \qquad (7)$$

where r and r' represent the position vectors for the observation point and the increment area dS', respectively, and u_0 and ε_0 denote the free-space permeability and permittivity, respectively.

The half-space Green's function has been introduced into the physical optics method to consider the scattering of electrically large conductive targets in half space. Combined with the graphical-electromagnetic computing (GRECO) method, the shadow regions have been previously removed by the hardware graphics accelerator, and the geometry information is obtained by reading the color and depths of each pixel.

To apply the far-field approximation, that is, the observation point is located far enough from the scattering object, we could substitute (2), (3) into the scattered field $\mathbf{E}_{sf}$ due to the facet's surface, which leads to the equation:

$$E_{sf}(\bar{r}) = -j\omega\int_s \bar{G}_A \cdot J(\bar{r}')ds' + \frac{k\cdot\hat{s}}{\omega}\int_s [G_x^{qe}\frac{\partial}{\partial x}J(\bar{r}') + G_y^{qe}\frac{\partial}{\partial y}J(\bar{r}') + G_z^{qe}\frac{\partial}{\partial z}J(\bar{r}')]ds' . \qquad (8)$$

Equation (8) is then calculated for every illuminated facet and the complex RCS due to scattering from every illuminated facet is calculated as [19]:

$$\sqrt{\sigma} = \lim_{R\to\infty} 2\sqrt{\pi}R\frac{E_{sf}\cdot\hat{e}_r}{E_o}\exp(jkR) , \qquad (9)$$

where $\exp(jkR)$ is a phase term that has been introduced into the equation in order to account for the facet location with respect to the global coordinate system. Here, R is the position vector for the facet's reference vertex with respect to the global coordinate system.

C. Wedge Scattering in Half-Space

According to the high-frequency method, the far field scattered from a wedge can be assumed as radiated by an equivalent line current located on the edge. This equivalent current depends on both the directions of incidence and observation relative to orientation of the edge, so that its value is not constant along the edge. F and V_m represent magnetic vector and scalar potentials.

The MEC (Method of Equivalent Currents) is an integrative technique dealing with radiation integrals. The source of the diffracted field is now ascribed to fictitious equivalent currents, both electric and magnetic currents flowing along the edge. This approach has been investigated by many authors. Here, the main formulations are presented. For detailed derivations, the interested reader may refer to [20-21]. The electric and magnetic equivalent currents can be represented as:

$$I_e = \frac{j2(\hat{t}\cdot E_{inc})D_e}{kZ_0\sin\beta_i\sin\beta_s} , \qquad (10)$$

$$I_m = \frac{j2(\hat{t}\cdot H_{inc})D_m}{kY_0\sin\beta_i\sin\beta_s} , \qquad (11)$$

where Y=1/Z is the admittance of the medium, and D_e, D_m is the soft, hard scalar diffraction coefficient [3].

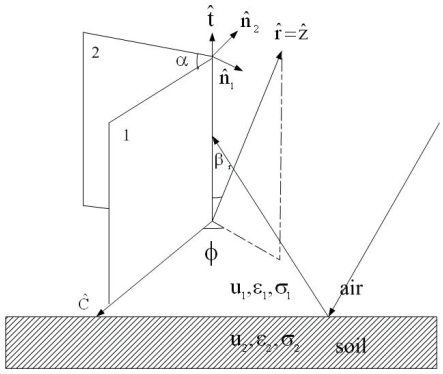

Fig. 5. The reflected field of the ground and wedge in half space.

The HFEEC (high-frequency equivalent electric current) depend on the angles α, ϕ, β_r, defined in Fig. 5. These angles were computed from the knowledge of the unit normal to both faces of the edge as follows:

$$\alpha = \cos^{-1}(-n_1.n_2) \ , \tag{12}$$

$$\sin\beta_r = \sqrt{t_x^2 + t_y^2} \ , \tag{13}$$

$$\cos\phi = \frac{n_{1x}t_y - n_{1y}t_x}{\sqrt{t_x^2 + t_y^2}} , \tag{14}$$

where t is the unit vector along the edge direction.

$$\hat{t} = \frac{n_1 \times n_2}{|n_1 \times n_2|} . \tag{15}$$

But it is not appropriate to calculate the scattering field from the ground by three-dimensional Green's function. In order to solve the scattering fields in half space, the half-space Green's function is introduced to calculate the contributions of scattering between the target and the ground plane.

As shown in Fig. 5, on the basis of the electric vector potentials, we consider the impact of the spatial domain half-space Green's function for the magnetic vector potentials.

$$\overline{\mathbf{G}}_{\mathbf{F}} = (\hat{\mathbf{x}}\hat{\mathbf{x}} + \hat{\mathbf{y}}\hat{\mathbf{y}})\mathbf{G}_{\mathbf{F}}^{\mathbf{xx}} + \hat{\mathbf{z}}\hat{\mathbf{x}}\mathbf{G}_{\mathbf{F}}^{\mathbf{zx}} + \hat{\mathbf{z}}\hat{\mathbf{y}}\mathbf{G}_{\mathbf{F}}^{\mathbf{zy}} + \hat{\mathbf{z}}\hat{\mathbf{z}}\mathbf{G}_{\mathbf{F}}^{\mathbf{zz}} \tag{16}$$

with

$$G_F^{xx} = G_F^{yy} , \tag{17}$$

where G_F^{xx}, G_F^{zx}, G_F^{zy} and G_F^{zz} denote the spatial domain half-space Green's function for the magnetic vector potentials;

It is permissible to express the vector and the scalar potentials as follows:

$$A_1(r) = \int_L \overline{G}_{A1}(r,r') \cdot I_e \hat{t} dL' \tag{18}$$

$$V_e(r) = \frac{-1}{j\omega\omega_0} \int_L [G_x^{qe}(r,r') I_e \frac{\partial t_x}{\partial x'} + G_y^{qe}(r,r') I_e \frac{\partial t_y}{\partial y'} + G_z^{qe}(r,r') I_e \frac{\partial t_z}{\partial z'}] dL' , \tag{19}$$

$$F_1(r) = \int_L \overline{G}_{F1}(r,r') \cdot I_m \hat{t} dL' \ , \tag{20}$$

and substitute (17), (18), (19) into the wedge scattered field E_{sw}.

$$E_{sw}(r) = -j\omega A(r) - \nabla V_e - \frac{1}{\varepsilon_0} \nabla \times F, r \in L . \tag{21}$$

Here, A and V_e represent electric vector and scalar potentials, F represents the magnetic vector potential, which leads to the equation:

$$\nabla \times \overline{\mathbf{G}}_F = \begin{bmatrix} \frac{\partial}{\partial \mathbf{y}} \mathbf{G}_F^{\mathbf{zx}} & \frac{\partial}{\partial \mathbf{y}} \mathbf{G}_F^{\mathbf{zx}} - \frac{\partial}{\partial \mathbf{z}} \mathbf{G}_F^{\mathbf{yy}} & \frac{\partial}{\partial \mathbf{y}} \mathbf{G}_F^{\mathbf{zz}} \\ \frac{\partial}{\partial \mathbf{z}} \mathbf{G}_F^{\mathbf{xx}} - \frac{\partial}{\partial \mathbf{x}} \mathbf{G}_F^{\mathbf{zx}} & -\frac{\partial}{\partial \mathbf{x}} \mathbf{G}_F^{\mathbf{zy}} & -\frac{\partial}{\partial \mathbf{x}} \mathbf{G}_F^{\mathbf{zz}} \\ -\frac{\partial}{\partial \mathbf{y}} \mathbf{G}_F^{\mathbf{xx}} & \frac{\partial}{\partial \mathbf{x}} \mathbf{G}_F^{\mathbf{yy}} & \mathbf{0} \end{bmatrix} . \tag{22}$$

The scattered electric field for the M illuminated wedge is defined as Equation (23) and the complex RCS due to scattering from every illuminated wedges is calculated as Equation (9).

$$\mathbf{E}_{sw}(\vec{\mathbf{r}}) = -j\omega\boldsymbol{\mu}_0 \int_L \overline{\mathbf{G}}_A(\mathbf{r},\mathbf{r}') \cdot I_e \hat{t} dL' + \frac{k \cdot \hat{s}}{\omega \cdot \varepsilon_0} \int_L [G_x^{qe} \frac{\partial}{\partial x} I_e \hat{t} + G_y^{qe} \frac{\partial}{\partial y} I_e \hat{t} + G_z^{qe} \frac{\partial}{\partial z} I_e \hat{t}] dL' - j\omega\varepsilon_0 \int_L \nabla \times \overline{\mathbf{G}}_F(\mathbf{r},\mathbf{r}') \cdot I_m \hat{t} dL'. \tag{23}$$

Therefore, the overall RCS for the complex body, assuming only first-order terms, is

$$\sigma = 4\pi \lim_{R\to\infty} R^2 \frac{\left| \sum_{n=1}^{N} (E_{sw} \cdot \hat{e}_r)_n + \sum_{m=1}^{M} (E_{sf} \cdot \hat{e}_r)_m \right|^2}{|E_o|^2} . \tag{24}$$

D. Multiple Scattering in Half-Space

Calculating the contributions of multiple scattering in half space is a formidable task. However, describing the complex geometry in terms of facets significantly reduces the problem. The multiple scattering contributions between the land and the targets are primarily expressed in terms of facet-facet interactions.

Multiple interactions between the target and the half-space interface are important when the target is near the interface. In the past, this issue is often ignored.

The field previously considered only incident is not enough, so the reflected field and the impact of multiple interactions must be taken into account. Consider a plane wave:

$$\vec{\mathbf{E}}_{\mathbf{i}}(\vec{r}) = \hat{\mathbf{q}} E_0 e^{-jk_0 \hat{\mathbf{i}}\cdot\vec{\mathbf{r}}}, \quad \hat{\mathbf{q}} = \hat{\mathbf{v}}_{\mathbf{i}}, \hat{\mathbf{h}}_{\mathbf{i}}, \tag{25}$$

where E_0 is the amplitude of incident field, $\hat{i}$ is the incident direction, and $\hat{v}_i, \hat{h}_i$ are the polarization vectors for incident electric and magnetic fields.

With

$$\hat{i} = \sin(\hat{x}\cos\varphi_i + \hat{y}\sin\varphi_i) - \hat{z}\cos\theta_i \quad , \tag{26}$$

$$\hat{h}_i = \frac{\hat{z}\times\hat{i}}{\left|\hat{z}\times\hat{i}\right|} = \hat{y}\cos\varphi_i - \hat{x}\sin\varphi_i \quad , \tag{27}$$

$$\hat{v}_i = \hat{h}_i \times \hat{i} = -\cos\theta_i(\hat{x}\cos\varphi_i + \hat{y}\sin\varphi_i) - \hat{z}\sin\theta_i . \tag{28}$$

The field can be calculated for orientation that is needed to study electromagnetic wave interaction with interface. The algorithm for this case is composed of two major steps.

1) Ray-tracing technique.

In order to apply the planar reflection coefficients reflection coefficients for the transverse electric (TE) Γ and the transverse magnetic (TM) case $\overline{\Gamma}$, the incident field needs to be decomposed into its TE and TM components. Using subscript c to denote local coordinates (see Fig. 6), the incident field can be written as:

$$E_1^i = (\vec{E}^i \cdot \hat{\phi}_c^i)\hat{\phi}_c^i + (\vec{E}^i \cdot \hat{\theta}_c^i)\hat{\theta}_c^i . \tag{29}$$

The reflected field is then given by

$$E_1^s = \Gamma(\vec{E}^i \cdot \hat{\phi}_c^i)\hat{\phi}_c^i + \overline{\Gamma}(\vec{E}^i \cdot \hat{\theta}_c^i)\hat{\theta}_c^i . \tag{30}$$

The reflected field is easily found once $\hat{\phi}_c^i$ and $\hat{\theta}_c^i$ are determined in terms of the global xyz coordinate in region I.

Once the ray paths from region I to region II are found, the field amplitude along the ray can be determined by geometrical optics [22]. Then, a ray-tracing technique is applied to the selected facet to compute the phase delay due to multiple bounce between the facets of the pair.

2) Physical Optical.

The multiple scattering contributions for selected facet in region II are computed by using a generalized form of Knott's calculations for an obtuse rectangular dihedral corner reflector [23]. His calculations were extended to account for the general case, in which the shape of the facet of the pair is quadrilateral or triangular. Computed contributions are then added to the overall fields in Equation (24).

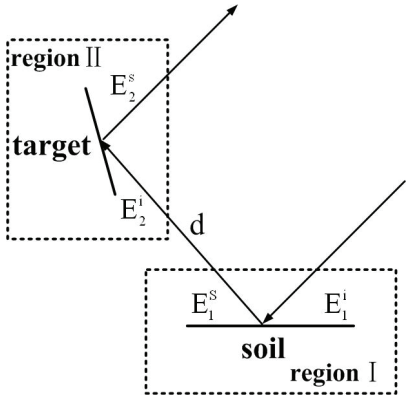

Fig. 6. The multiple scattering between the ground and target in half space.

III. RESULTS

When the object is calculated with the high-frequency method from the simple targets to the complex ones in half space, the CPU time for the RCS prediction is spent only on the electromagnetic part of the computation while the more time-consuming geometric model manipulations are left to the graphics hardware. Regardless of whether the targets are simple or complex ones, the scattering field of each illuminated pixel is calculated in the same way. Combined with the half-space Green's function, the high-frequency approximations to RCS prediction is easily computed from the knowledge of the unit normal at the illuminated targets in half space.

If we consider the simulation of complex electrically large size ($l >> \lambda$) targets with HFSS software, it is very easy to exceed the existing computer memory space, so we first compare with the results of the calculation and the simulation of the simple electrically large size targets in half space, and apply this algorithm to the complex ones in half space.

To ensure correlation with computations, special attention was given to the accuracy of model construction. Illustrations of the verification work are presented in the following sections.

A. Half Space and Free Space

Figure 7 shows a perfectly conducting pyramid ($5\lambda \times 5\lambda \times \lambda$) is placed $\lambda/4$ above the soil. Here, λ represents the wavelength in the vacuum. The soil has a relative dielectric permittivity $\varepsilon_r = 4.0$, relative magnetic permeability $\mu_r = 1.0$. The agreement is excellent.

There is good fit between the prediction of the derivation equation and the simulation of HFSS software, but there are slight discrepancies in some places. The major reason is the phase term that has been introduced into the equation to account for the facet location with respect to the global coordinate system.

Figure 8 shows a perfectly conducting ellipsoid is placed $\lambda/4$ above the soil. Here, the soil has a relative dielectric permittivity $\varepsilon_r = 4.0$, relative magnetic permeability $\mu_r = 1.0$.

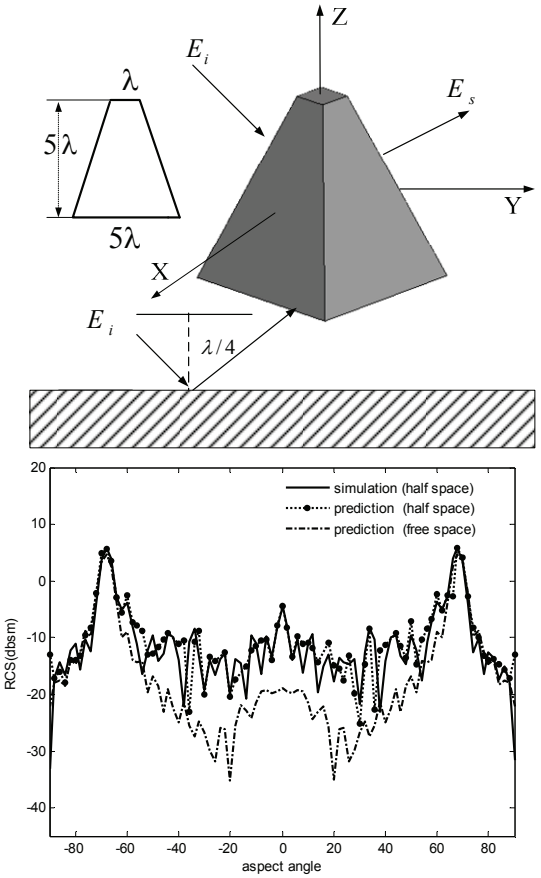

Fig. 7. 5 λ *5 λ *1 λ pyramid comparison of prediction and simulation of software in half space, frequency 10 GHZ, vertical polarization.

We can conclude that it is necessary to consider the effect of the half space environment. The results show that the RCS calculated with half-space Green's function are greater than that calculated with free-space Green's function. Compared with the actual results, it is efficient and accurate to introduce the half-space Green's function into the conventional the high-frequency method.

B. Wedge Scattering

Figure 8 shows a perfectly conducting wedge placed $\lambda/4$ above the soil. Here, the soil has a relative dielectric permittivity $\varepsilon_r = 4.0$, relative magnetic permeability $\mu_r = 1.0$.

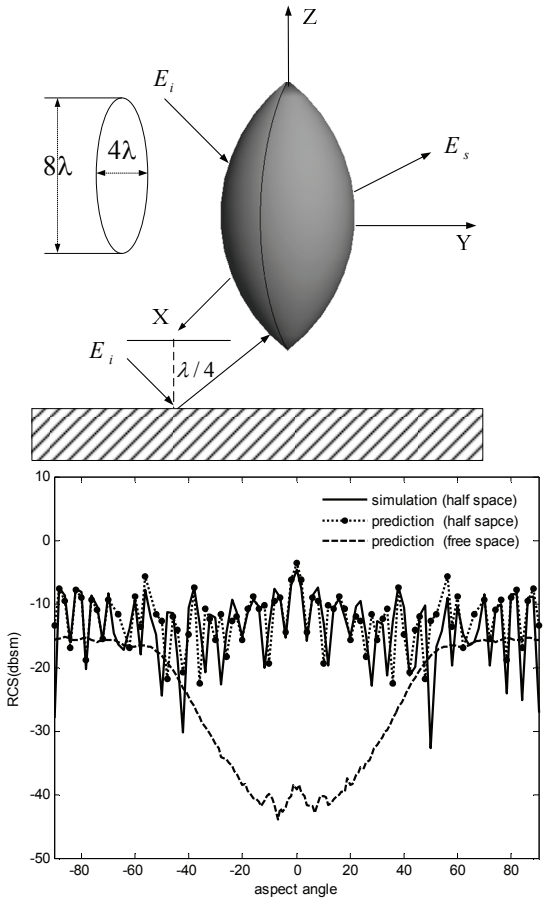

Fig. 8. 8 λ *4 λ ellipsoid comparison of prediction and simulation of software in half space, frequency 10 GHZ, vertical polarization.

It indicates the predictions are in good agreement with the simulation of software, which proves that the half-space Green's function applied the wedge is accuracy for the targets with large electric

dimensions in half space. In Fig. 9, We could see that, for these backscatter RCS, inclusion of returns from these wedges in the overall return is an important process.

C. Multiple Scattering

Figure 9 shows a perfectly conducting ellipsoid placed $\lambda/4$ above the soil. Here, the soil has a relative dielectric permittivity $\varepsilon_r = 4.0$, relative magnetic permeability $\mu_r = 1.0$.

It is important to notice that in Fig. 10, the multiple scattering in half space (HFMUL) is correct for aspect angles between -30^0 to -10^0 and 10^0 to 30^0. In order to improve the high-frequency result, the method of HFMUL is added to HFPO + HFEEC, the numerical solution agrees very well with the simulation results.

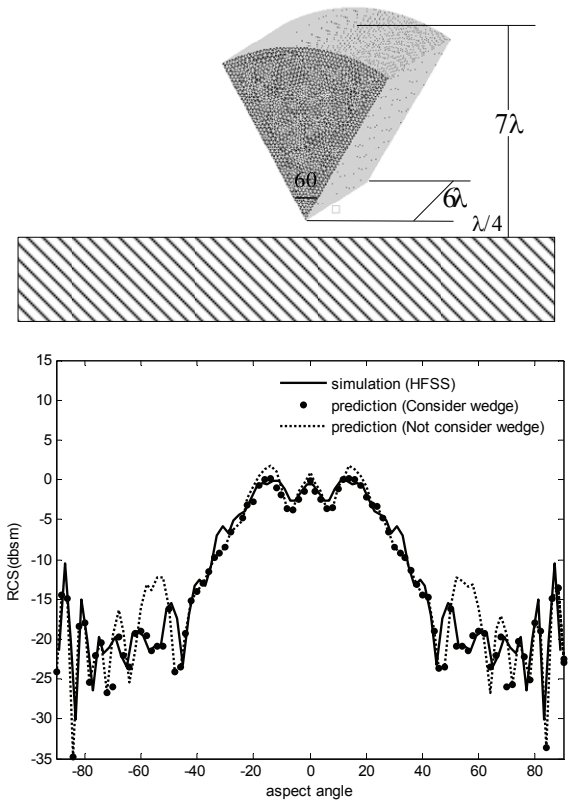

Fig. 9. Wedge comparison of prediction and simulation of software in half space, frequency 10 GHZ, vertical polarization.

D. Complex Targets

Various complex bodies have been used for verifications. The following presents an illustration for a generic missile model. Figure 11 shows the missile is placed 5m above the soil. The soil has a relative dielectric permittivity $\varepsilon_r = 4.0$, relative magnetic permeability $\mu_r = 1.0$.

Figure 12 shows that the contributions of scattering between the target and the ground plane have a great effect upon the predictions in half space. The prime reason for that is the phase discrepancy caused by the reflected waves with different wave distance from the ground and the scatters. In fact, the scattering fields in half space may be easily found for a set of source, if the half space dyadic Green's function of the environment are available [15].

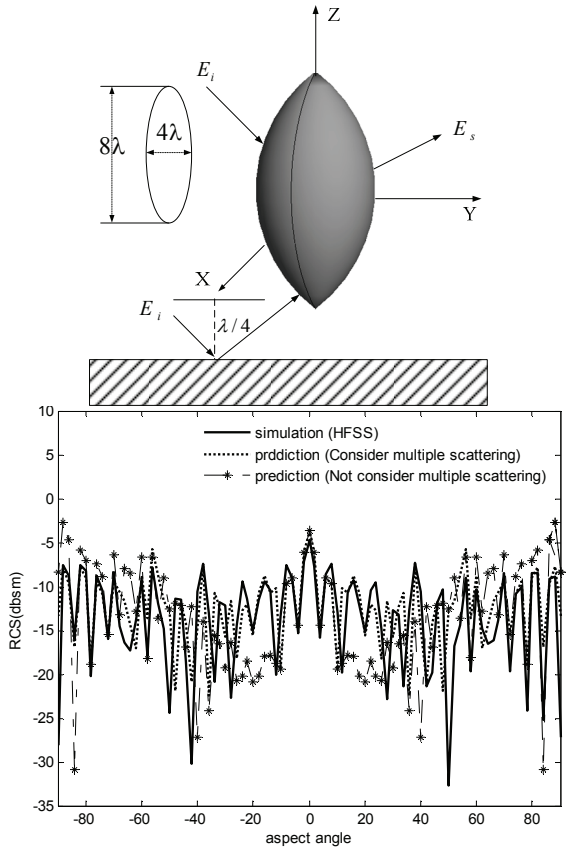

Fig. 10. The ellipsoid is placed $\lambda/4$ m in half space, frequency 10 GHZ, and vertical polarization.

IV. CONCLUSION

In this paper, we have presented an accurate and efficient approach for calculating the electrically large PEC targets in half space. In order to consider the electrically large PEC targets in half space, the half-space high-frequency method has been deduced by introducing the half-space Green's function into the conventional physical optics method (PO), method of equivalent currents (MEC). Combined with the graphical-electromagnetic computing (GRECO) method, the shadow regions are eliminated by displaying lists technology of OpenGL to rebuild the target and the geometry information is obtained by reading the color and depths of each pixel. Finally, we included the correction in our calculations by accounting for the currents on facets that were illuminated by the ground reflected wave. Then one may calculate the radar cross-section of a conductive target object in a half space. The numerical results have shown that this method is efficient and accurate.

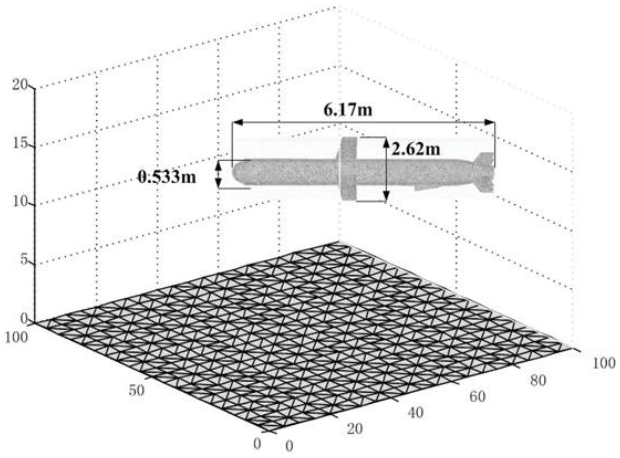

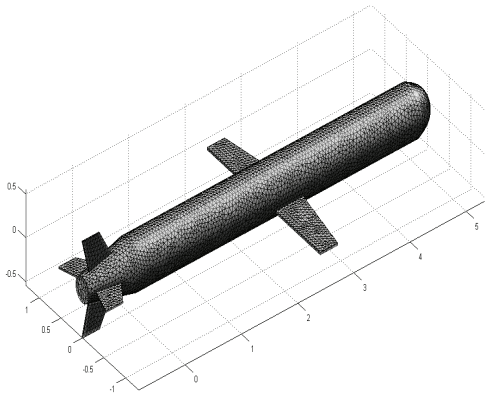

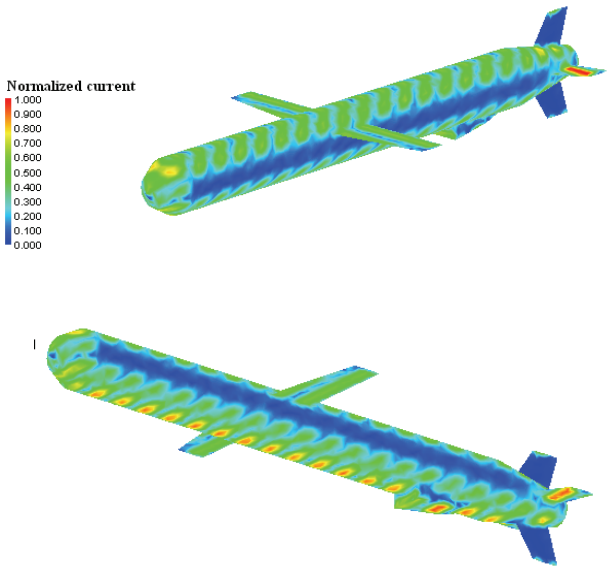

Fig. 11. Induced electric current on the surface of the missile in half space, frequency 1 GHZ, vertical polarization, at a incident angle of $\theta_i = 30, \varphi_i = 0$.

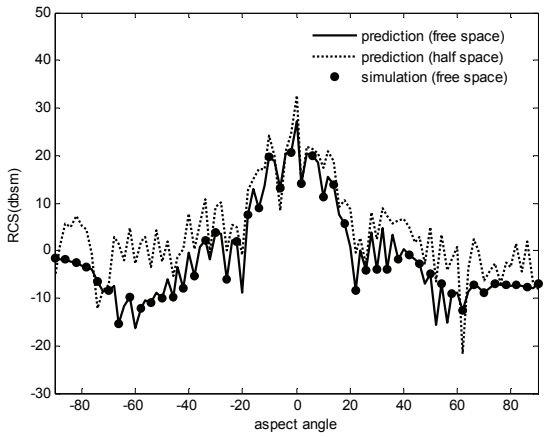

Fig. 12. The missile is placed 5m above the soil in half space, frequency 1 GHZ, and vertical polarization.

REFERENCES

[1] N. Yousee, "Radar Cross Section of Complex Targets," *Proc. IEEE*, vol. 77, no. 5, pp. 722-734, 1989.

[2] D. M. Elking, J. M. Roedder, D. D. Car and S. D. Alspach, "A review of high-frequency radar cross section analysis capabilities at McDonnell Douglas aerospace," *IEEE Antennas and Propag*, vol. 37, no. 5, pp. 33-43, 1995.

[3] J. M. Rius, M. Ferrando and L. Jofre, "High-Frequency RCS of complex radar targets in real-time," *IEEE Antennas and Propag,* vol. 41, no. 9, pp. 1308-1460, 1993.

[4] E. F. Knott, "A Progression of high-frequency RCS prediction techniques," *Proc. IEEE,* vol. 73, pp. 252-264, 1985.

[5] C. Long Yu and S. W. Lee, "Radar Cross Section Computation and Visualization by Shooting and Bouncing rays (SBR) Technique," *IEEE Antennas Propag,* vol. 37, pp. 194-205, Feb. 1989.

[6] S. M. Rao, D. R. Wilton, A. W. Glisson, "Electromagnetic scattering by surfaces of arbitrary shape," *IEEE Trans. Antennas Propag*, vol. 30, pp. 409-418, 1982.

[7] M. Domingo, F. Rivas, J. Perez, R. P. Torres, and M. F. Catedra, "Computation of the RCS of complex bodies modeled using NURBS surfaces," *IEEE Antennas Propag*, vol. 37, no. 1, pp. 36-47, 1995.

[8] D. H. Han and A. C. Polycarpou, "Ground Effects for VHF/HF antennas on helicopter air frames," *IEEE Trans Antennas Propag*, vol. 49, no. 3, pp. 402-412, 2001.

[9] Q. L. Li, D. B. Ge, S. Y. Shi, and Y. B. Yan, "An Approach for Solving Ground Wave Scattering from Objects," *J. MICROW,* vol. 14, no. 3, pp. 23-28, 1998.

[10] X. L. Ming, N. Z. Ping, and W. Jun, "Electric-Field-Type Dyadic Green's Functions for Half-Spaces and its Evaluation," *J.UEST China,* vol. 33, no. 5, pp. 485-4881, 2004.

[11] Z. Liu, J. He, Y. Xie, A. Sullivan, and L. Carin, "Multilevel Fast Multiple Algorithm for General Targets on a Half-Space Interface," *IEEE Trans. Antennas Propag,* vol. 50, no. 12, pp. 1838-1849, 2002.

[12] J. T. Johnson, "A study of the four-path model for scattering from an object above a half space," *Microwave and Optical Technology Letters*, vol. 30, no. 2, pp. 130-134, 2001.

[13] X. F. Li, Y. J. Xie, P. Wang, and T. M. Yang, "High-Frequency Method for Scattering From Electrically Large Conductive Targets in Half-Space," *IEEE Antennas and Wireless Propagation Letters*, vol. 6, pp. 259-262, 2007.

[14] X. F. Li, Y. J. Xie, and R. Yang, "High-frequency method analysis on scattering from homogenous dielectric objects with electrically large size in half space." *Progress in Electromagnetic Research B,* vol. 1, pp. 177-188, 2008.

[15] J. J. Yang, Y. L. Chow and D. G. Fang. "Discrete complex images of a three-dimensional dipole above and within a lossy ground," *Proc. Inst. Elect. Eng. H*, vol. 138, no. 4, pp. 319-326, 1991.

[16] Y. L. Chow, "A closed-form spatial Green's function for the thick microstrip substrate," *IEEE Trans. Microwave Theory Tech*, vol. 39, no. 3, pp. 588-592, 1991.

[17] G. Dural and M. I. Aksum, "Closed-Form Green's Function for General Sources and Stratified Media," *IEEE Transaction on Microwave Theory and Techniques*, vol. 43, no. 7, July 1995.

[18] M. I. Aksum, "A Robust Approach for the Derivation of Closed-Form Green's Function," *IEEE Transaction on Microwave Theory and Techniques*, vol. 44, no. 5, May 1996.

[19] Y. Z. Ruan, *Radar Cross Section and Stealth Technology,* National Defense Industry Press, 1998.

[20] A. Michaeli, "Equivalent edge currents for arbitrary aspects of observation," *IEEE Trans. Antennas Propag*, vol. 32, pp. 252-258, 1984.

[21] A. Michaeli, "Elimination of infinities in equivalent edge currents, part I: Fringe current components," *IEEE Trans. Antennas Propag*, vol. 34, pp. 912-918, 1986.

[22] H. Ling, R. C. Chou, and S. W. Lee, "Shooting and Bouncing Rays: Calculating the RCS of an Arbitrarily Shaped Cavity," *IEEE Trans. Antennas Propag*, vol. 37, pp.194-205, 1989.

[23] E. F. Knott, "RCS reduction of dihedral corners," *IEEE Trans. Antennas Propag*, vol. 25, pp. 406-409, May 1977.

Xiao Feng Li received the Bachelor degree in electronic engineering from Xidian University, Xi'an, Shannxi, China, in 2005. Since 2006, he has taken a combined master-doctor program and worked

for Ph.D. in Xidian University. He has been engaged in the development of the high-frequency RCS predictions. His current research interests involve both high frequency techniques and numerical methods for electromagnetic scattering analysis.

Yong Jun Xie received the B.S., M.S., and Ph.D. degrees in electronic engineering from the Xidian University, Xi'an, Shannxi, China, in 1990, 1993 and 1996, respectively. From 1998 to 1999 he worked at the University of Texas at Dallas as a postdoctoral research associate. Then he worked at Duke University as a postdoctoral research associate from 1999 to 2001. Currently he is a professor at Xidian University. His research interests include electromagnetic theory, microwave technology, and mobile telecommunications.

Rui Yang received the Bachelor degree in electronic engineering from Xidian University, Xi'an, Shannxi, China, in 2004. Since 2005, he has taken a combined master-doctor program and worked for Ph.D. in Xidian University. His current research interests involve metamaterials and antenna design.

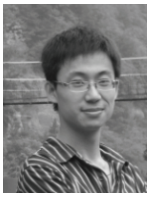

Yuan Yuan Wang received the Bachelor degree in electronic engineering from Xidian University, Xi'an, Shannxi, China, in 2005. Since 2006, he has taken a combined master-doctor program and worked for Ph.D. in Xidian University. His current research interests involve metamaterials and antenna design.